Laboratory Testing of a Modular 8-Thruster Scalable Ion Electrospray Propulsion System

IEPC-2017-062

Andrea G. Hsu[1], Brian B. Brady[2], Myriam P. Easton[3], Aura C. Labatete-Goeppinger[4],Thomas J. Curtiss[5]
The Aerospace Corporation, El Segundo, CA 90245, USA

and
David Krejci[6], Paulo Lozano[7]
Space Propulsion Laboratory, Massachusetts Institute of Technology, Cambridge, MA 02139, USA

Abstract: The lifetime performance of an 8-thruster scalable ion electrospray propulsion system module was assessed. The propellant was EMI-BF_4 ionic liquid. The lifetime of the thrusters was 40 hours operating at a nominal current of approximately 600 µA per polarity (1200 µA total for 8 thruster heads), limited by thruster shorting and subsequent arcing. Warm-up/conditioning occupied a 3–4 of the 40 hours. A maximum of 74 µN of thrust was produced by the 8 thrusters. The thrusters required concurrent equal and opposite operating voltages to charge-neutralize and operate nominally. The emitted current and thrust were recorded in real time as a function of the applied voltage over the lifetime of the thruster unit at emitted currents ranging from 100 to 650 µA. A best linear fit of 70 nN thrust per µA of emitted current was observed. These thrusters were configurationally very similar to ones tested previously in 2014, but demonstrated vastly improved performance and behavior, reflecting advancements in thruster design and manufacturing.

Nomenclature

T	=	thrust (Newtons)
θ	=	deflection (radians)
k	=	spring constant (N*m/rad)
L	=	moment arm (m)
F	=	force (Newtons)
V	=	voltage bias (V)
D	=	electrode separation (m)
A	=	electrode surface area (m^2)

[1] Research Scientist, Propulsion Science Department, 2310 East El Segundo, Mailstop M2-341.
[2] Senior Scientist, Propulsion Science Department, 2310 East El Segundo, Mailstop M2-341.
[3] Senior Scientist, Materials Science Department, 2310 East El Segundo, Mailstop M2-242.
[4] Analytical Chem. Spec., Materials Science Department, 2310 East El Segundo, Mailstop M2-242.
[5] Director, Propulsion Science Department, 2310 East El Segundo, Mailstop M2-341.
[6] Research Scientist, Aeronautics and Astronautics, 77 Massachusetts Avenue, Mailstop 37-401
[7] Professor and Director of SPL, Aeronautics and Astronautics, 77 Massachusetts Avenue, Mailstop 37-401

I. Introduction

CUBESATS, small lightweight satellites satisfying the cubesat design protocol [1], are becoming increasingly popular space vehicles due to their low cost and simplicity. The combination of relatively low launch costs, rapid development cycles and the possibility for constellations at low cost, featuring redundancy, high temporal resolution and flexibility, have resulted in a fast growing number of Nanosatellite missions [2].One factor limiting the utility of CubeSats is the lack of an efficient propulsion system for this class of satellite. The lack of propulsion, combined with a dearth of dedicated CubeSat launchers, means CubeSats are often stuck in less than ideal orbits for a given mission. One approach to improving this situation is the development of a miniature ion Electrospray Propulsion System; the proposed system could potentially use less than 30% of the volume of a 1U CubeSat [3].

The electric propulsion system, an ion electrospray thruster, will be referred to as a **S**calable **i**on **E**lectrospray **P**ropulsion **S**ystem (S-iEPS) in this report. The S-iEPS unit was developed and built by MIT Space Propulsion Laboratory for NASA's Micro Electrospray Propulsion (MEP) program. Direct thrust measurements were carried out at The Aerospace Corporation using a torsional micro-newton thrust stand. Ground thrust measurements will be crucial both towards understanding thruster performance on orbit, as only limited telemetry will be available for monitoring thruster operating conditions in flight, and for designing future missions using S-iEPS.

The working principle behind ion electrosprays is based on the electrostatic extraction and acceleration of positive and negative ions and/or ion clusters from an ionic liquid propellant—an extremely low vapor-pressure conductive salt that remains in the liquid phase at room temperature and within the temperature range typical of a small satellite (approximately -10 to 300 C) [4]. Although many candidate ionic liquids exist, EMI-BF_4 was chosen for this test campaign due to its non-toxicity and other physical properties (viscosity, conductivity, density). In order to extract these ions and ion clusters, intense electric fields such as those found at the tip of electrically stressed Taylor Cones are required [5]. Taylor Cones, which have sizes from a fraction to several micrometers, can be produced at the end of sharp emitter structures, such as sharpened capillaries or needles biased with respect to a downstream extractor aperture.

The thrust obtainable from single electrospray emitters is too small for most practical applications. As such, there is a need to build dense arrays of emitters that would fire in parallel [6-10]. However, to make the thruster system useful for small satellites, such arrays of emitters need to be contained within a compact footprint. This can be achieved using Micro Electro Mechanical Systems (MEMS) materials and processes and a passive propellant feed system. Emitters are fabricated on porous materials, so that propellant can flow via capillarity through the bulk of the material. Since the propellant is passively drawn to the thruster face, bulky propellant delivery hardware such as pressurized vessels and valves is not needed.

S-iEPS thrusters consume <1W of power while firing, and are highly **scalable, limited primarily by available spacecraft power**. Scaling could be performed at the device level, by increasing the density of emitters of a single thruster module, or at the system level, by adding modules of a fixed density in parallel configurations (offering inherent risk reduction via redundancy). In its most beneficial implementation, both approaches would be combined to construct "flat-panel thrusters" including propellant management and electronics in a high-performance propulsion system that would be significantly smaller and less massive than options available today. Because of its modular nature, the S-iEPS system is ideally suited for rapid technology development on CubeSats and small satellites, towards potential applications on large satellites with little or no required system modifications.

This report details the thruster characterization testing that was completed on a single 8-thruster S-iEPS unit and represent the first known direct thrust measurements on the system. These ground data would be essential for comparing to any potential on-orbit performance data. This report also intends to provide an independent evaluation of MIT's S-iEPS technology to give the community a sense of the technology's readiness and evolution for transfer to a third party. The results of this testing have been summarized briefly in [13], and this report provides further details on the direct thrust measurements reported in [13]. The experimental goals were to (1) become familiar with the operation of the thrusters, (2) operate the thrusters for as long as possible, and (3) collect performance data (emitted current and thrust) over the thrusters' lifetime.

II. S-iEPS Test Article

The MIT S-iEPS system is a MEMs-based thruster that uses EMI-BF_4 as its ionic liquid propellant. The thruster utilizes a PEEK plastic tank, capped with a porous glass emitter substrate, which consists of 480 microscopic emitters. The propellant is housed within the plastic tank and the porous substrate, and is contained via capillary forces. No

pressurized tanks or valves are needed. To operate the thruster, an electrode within the propellant reservoir (distal electrode) is biased to high voltages relative to the extraction grid above the emitter substrate. This voltage bias causes ions to be emitted through the extraction grid, producing thrust. The voltage of the distal electrode is switched from positive polarity to negative polarity, both to preserve electrical neutrality of the propellant within the reservoir, and thruster plume neutrality [11,12]. A single thruster occupies 14.4 mm (W) x 14.4 mm (D) x 14.1 mm (H) and contains 1.2 cm3 of propellant. The S-iEPS unit carried 8 of these thrusters all designed to fire along a single axis. The weight of the S-iEPS unit was 100g, including the PPU. A more detailed discussion of the S-IEPS test article can be found in [13] and additional characterization in [14].

Electrical Configuration

All 8 thrusters were connected on a single "channel." That is, all 8 extractor grids were connected to the PPU ground, allowing them to float to approximately +/-200V with respect to the low voltage side PPU ground. Four of the distal electrodes were connected and could be biased to one particular voltage (either positive or negative), and the other four were connected in the same fashion in a checkerboard pattern. Therefore, all thrusters had to be fired concurrently; thrusters could not be commanded independently. Although it was possible to fire four of the thrusters and not the other four, operating in this manner caused the unit to charge up and did not produce appreciable thrust. Data will be shown addressing this issue. This electrical configuration simplified the PPU since fewer HV switches were required, giving the S-iEPS an extremely compact total footprint of <0.2U (<200 cm3). Only a single electrical board was required to operate the system. However, it also meant that a single short in any one thruster would end the lifetime test. More recent thruster units offer redundancy via independent channel control while preserving a compact footprint using smaller switches. A photograph of the thruster unit is shown in Figure 1 [14]. The left image shown the thrusters mounted on the single-board PPU. The right image shows the unit with a protective enclosure, ready for testing. The unit is <0.2U (Reference 3 with permission from MIT). Four electrical leads originating from the S-iEPS were prepared, two that were routed to the PPU for normal operation, and two that bypassed the PPU to power the thrusters directly. As a backup, laboratory high-voltage units were available which could bypass the PPU and power the thrusters directly, coupled with in-house Labview DAQ software.

III. Thrust Stand and Experimental Setup

The thrust stand used to characterize thruster performance is based on a torsional design and consists of a rigid aluminum arm, balanced atop a frictionless pivot with a calibrated spring constant. The thruster is mounted on one side of the arm, and counterweights are used to balance the arm on the opposite side. When the thruster fires, the arm is displaced, and the displacement is measured via an optical displacement meter; the thrust is calculated directly from the resulting displacement and the known spring constant. The thrust stand's sensitivity is better than 1 μN. Details on the thrust stand design, calibration, and measurement resolution are provided in [15]. The main arm of the thrust stand is made of rectangular aluminum tubing to save weight while maximizing rigidity. The pivot spring constant is nominally 0.0279 in*lb/deg (Riverhawk Industries, axial load limit =38 lbs) and is held in place by custom stainless-steel mounts. The thrust stand is calibrated using known electrostatic forces between a pair of bare aluminum electrodes, shown on the left side of the thrust stand. The electrodes are held far from the thrust stand body to minimize fringing effects. A delrin flag attached to the back of the larger electrode which holds a small (7 mm dia) mirror and is the target for the optical displacement meter (Philtec). The optical displacement meter directly measures the displacement of the thrust stand arm. The moment arms for the electrodes and the optical displacement meter are equivalent (23 cm), and the moment arm to the thruster is 12.7 cm.

Thrust in a torsional-type thrust stand is calculated directly from Eq. (1):

$$T = \frac{\theta * k}{L} \tag{1}$$

Where T is thrust (Newtons), θ is the deflection of the arm (radians), k is the spring constant (N*m/rad), and L is the moment arm (m). In this case, θ is measured directly via the optical displacement meter. The spring constant is estimated by the manufacturer, but the exact value was measured. To experimentally measure k, calibration electrodes were utilized to exert a known electrostatic force on the thrust stand. The calibration electrodes were made of bare aluminum and had 0.75 in. and 2 in. diameters. The 0.75-in. electrode was mounted to a translational stage and the 2-

in. electrode was mounted to the thrust stand. One electrode has a larger diameter than the other to minimize fringing effects. Given a known bias between the electrodes, the force could be calculated from Eq. (2) for a parallel-plate capacitor:

$$F = \frac{1}{2}\varepsilon_0 \left(\frac{V}{D}\right)^2 A \qquad (2)$$

Where F is force (Newtons), V is the voltage difference, D is the electrode separation, and A is the surface area, in this case, of the smaller electrode. However, the force was experimentally measured using a microbalance (and compared to the calculated value) for increased measurement accuracy.

The S-iEPS thruster's four leads were wired using 36 gauge bare copper wires to minimize forces on the thrust stand arm. A photograph of the S-iEPS unit mounted to the thrust stand is shown in Figure 2. In this photo, the electrostatic calibration electrodes are near the left side. Counterweights were used to balance the thruster unit, and a passive damper was located on the right end of the thrust stand. Electrostatic calibration was completed as described in [4] and yielded that 1 μm of thrust stand arm displacement is equal to 8.2 μN of thrust. The small residual forces caused by the electrical leads were accounted for by calibrating the thrust stand with the wires in place. The vacuum chamber was approximately 5' long and 3' in diameter. It had a baseline pressure of approximately 4*10-7 Torr and was pumped by 2 roughing pumps and three Leybold turbopumps for a total pumping speed of 2850 lps. The thruster was visible through a viewport on the front of the chamber.

IV. Test Results and Discussion

Upon arrival at The Aerospace Corporation from MIT, the test article was visually and electrically inspected. Laboratory power supplies and DAQ system were used due to PPU malfunctions. Four of the emitters were controlled by one high-voltage supply, and the remaining four were controlled by the other in a checker-board pattern. The extracted current could not be measured in this setup because the extractors were routed through the malfunctioning PPU. The recommended maximum current draw was 150 μA per thruster. We knew that the thruster's warm-up period was critical from previous testing, so a gentle warm-up routine was employed, consisting of the following steps:

> (1) Power half of the thrusters at a positive voltage and the other half with negative voltage. Ramp up voltage in non-switching mode slowly up to operating voltage, pausing to allow current to stabilize at each voltage
> (2) Switch polarities and do the same as (1)
> (3) Manually implement switching mode, again pausing at each voltage to allow current to stabilize. At high voltages, pause for many minutes to ensure current is stable. Switch many times at the operating voltage to ensure thruster can implement voltage without current instabilities. Do not switch faster than 30s per polarity.
> (4) Implement automatic user profile, again ramping up to operating voltage gently. Do not switch faster than 30s per polarity.

The thruster was first slowly ramped up to positive voltage via one of the leads, and the other was left grounded. This produced very little thrust and emitted current, even at extremely high voltages. For example, at 1500 V, only ~140 μA and ~10–15 μN were observed. Identical behavior was observed in the negative direction. The thruster only began to operate nominally when one lead was ramped in the positive direction and the other was ramped in the negative direction concurrently. This suggests that the thrusters require nearly equal and opposite operating emitted currents to charge-neutralize, which again emphasizes the importance of operating the thrusters in opposite-polarity pairs. The manual data for steps 1–3 is shown in Figures 3 and 4. The right axis shows the raw displacement data (optical displacement meter, or ODM) and is not converted to thrust because of the naturally thermally drifting baseline. The data traces are "T1 Iemit (uA)" and "T2 Iemit (uA)" which are the emitted currents for thruster channels 1 and 2, respectively. Similarly, "T1 Volt" and "T2 Volt" refer to the commanded voltages. Interesting aspects of thruster behavior are denoted in the figures. In Figure 4, "A" shows the thrust stand drifting, likely the result of charging, when the thruster was not producing thrust. At "B", both positive and negative polarities are engaged, and the thruster began to operate nominally. "C" shows normal thruster operation, and thrust was produced. "D" again shows similar behavior as "A", thruster instabilities at low voltages when no propellant is being emitted. At about

800V, the thrust began to start up, and was operating nominally by ~1000V. At the end of this test, the thruster was commanded to 0V to begin an automatic switching profile. The base pressures were $5*10^{-7}$ Torr for measurements shown in Figures 3 and 4. The voltage was periodically commanded to 0 V to establish a thrust stand baseline.

Once the thrusters were fully conditioned on manual control (about 4 hours into thruster operation), a user profile was uploaded to ramp the thrusters to 1075V, in switching mode (switching polarities every 30 seconds), where it operated in a mostly stable manner. A closeup of this data is shown in Figure 5. "G" and "H" denote examples intermittent shorts, both of which cleared on their own. The automated profile simulated the gradual warm-up of the manual operation profile, and was characterized by overall stable operation with a few intermittent shorts. Close to the thruster's end of life, these were seen more frequently. The thruster encountered a permanent short at 40 hours, ending the lifetime test. A plot of thrust vs. emitted current showed an expected linear relationship (Figure 6) of approximately 70 nN per μA emitted current. The points at 32 and 37 hours also show that the thruster performance degraded slightly over time. The data from this report is summarized in [13].

Post-life visual inspection and chemical analysis

Microscope images of the thruster after the test are shown in Figures 7-9. Every thruster showed at least a few black marks on the emitter surface indicative of decomposed propellant "tar" from firing and/or intermittent arcing. The top right thruster's grid fell off, which likely ended the life test. We hypothesize that an arc led to high levels of local heating, which then melted the epoxy that held the grid onto the thruster. The lower left corner of that thruster was completely burned, and may have been the arc location. Two of the neighboring thrusters had liquid shorts, which appear as bright, glistening grid openings such as in inspection image 6 in Figure 8. The remaining thrusters showed wear ranging from heavily fired (many black marks and propellant "tar" buildup on the grids such as thruster 7 in Figure 7) to relatively clean (thruster 6 in Figure 7). Inspection images 26 and 27 in Figure 9 show the propellant "tar" buildup spike that started from the extractor grid and grew towards the emitter. These variations in thruster wear suggested that the thrusters may have been drawing different amounts of current (i.e. producing varying amounts of thrust). The thruster current draw is highly sensitive to many factors including emitter tip geometry, distance from the extractor grid, propellant transport through the porous medium (i.e. pore size), emitter surface coating(s), thruster cleanliness, quality of electrical connections, etc. These tests have been fundamental to understand the nature of these variations and guide current efforts to improve the quality and uniformity of materials and manufacturing methods.

The thruster unit deposited a brown film on surfaces within the plume of the thrusters which was sent for chemical analysis. Such analysis is crucial for assessing potential spacecraft contamination on surfaces like optics and solar cells. Fourier transform infrared spectroscopy (FTIR) was collected using an attenuated total reflectance (ATR) attachment on a Thermo Nicolet 6700 Spectrometer. The sample was applied directly to the diamond window. A total of 150 scans were collected using a deuterated triglycine sulfate (DTGS) detector and 4 cm^{-1} resolution setting. This chemical analysis showed that many of the peaks matched with that of literature EMI-BF_4 spectra, suggesting that there was EMI-BF_4, perhaps from droplet accumulation, within the deposit. This is of particular concern because of the propellant's nearly zero vapor pressure; once the propellant adsorbs to a spacecraft surface, there is no viable removal mechanism. Droplet emission is a symptom of anomalously high flow rate allowed by the propellant management system, which is partly controlled by the pore size and porosity of the substrate material. Recent development efforts include research on alternative materials that improve overall uniformity while allowing these thrusters to operate in the pure ionic mode where droplet emission is completely suppressed [16].

V. Conclusions

A scalable 8-thruster ion electrospray propulsion system (S-iEPS) thruster module was characterized through a lifetime test. The thrusters performed well, demonstrating large improvements both in electrical behavior and lifetime compared to previous test units. The lifetime of the module was 40 hours at 600 μA nominal current, limited by thruster arcing of a suspected single thruster. Proper thruster warm-up and spacecraft neutralization were essential for nominal operation. Post-life system inspection revealed that the degree to which each thruster was fired varied, suggesting that the thrusters may have been drawing different amounts of current (i.e., producing varying amounts of thrust). Spacecraft contamination may be a potential concern. These test results have guided existing efforts that improve the performance and lifetime characteristics of electrospray thrusters.

Acknowledgments

The authors would like to acknowledge Fernando Mier-Hicks (MIT Space Propulsion Laboratory) and Espace Inc. (Francois Martel) for their support during the testing campaign. This work was supported by NASA through contract No. NNL13AA12C under NASA's Game Changing Development program of the Space Technology Mission Directorate (STMD).

References

[1] CubeSat Design Specification Rev. 13, California State Polytechnic University. Retrieved 2014-07-07.
[2] Selva, D., Krejci, D., "A survey and assessment of the capabilities of cubesats for earth observation," Acta Astronautica, 74(0):50-68, 2012.
[3] Ion Electrospray Propulsion System for CubeSats (iEPS), Space Propulsion Laboratory, Massachusetts Institute of Technology. Retrieved 2014-07-10.
[4] Smith, E., Rutten, F., Villar-Garcia, I., Briggs, D., License, P., "Ionic liquids in vacuo: analysis of liquid surfaces using ultra-high-vacuum techniques," Langmuir, 22(22):9386-9392, 2006.
[5] Romero-Sanz, I., Bocanegra, R., Fernandez de la Mora, J., Gamero-Castano, M., "Source of heavy molecular ions based on Taylor cones of ionic liquids operating in the pure ion evaporation regime," Journal of Applied Physics, Volume 94 (5), 2003.
[6] Arscott, W., Le Gac, S., Druon, C., Tabourier, P., Rolando, C., "Micromachined 2d nanoelectrospray emitter [mass spectrometer applications]. Electronics Letters, 39(24):1702-1703, 2003.
[7] Gassend, B.L.P. A Fully Microfabricated Two-Dimensional Electrospray Array with Applications to Space Propulsion. PhD thesis, Massachusetts Institute of Technology, 2007.
[8] Courtney, D., Hanqing Q., Lozano, P., "Emission measurements from planar arrays of porous ionic liquid ion sources," Journal of Physics D: Applied Physics, 45(48):485203, 2012.
[9] Spindt, C., "Microfabricated field-emission and field-ionization sources," Surface Science, 266(1-3):145-154, 1992.
[10] Tang, K., Lin, Y., Matson, D., Kim, T., Smith, R., "Generation of multiple electrosprays using microfabricated emitter arrays for improved mass spectrometric sensitivity," Analytical Chemistry, 73(8):1658-1663, 2001.
[11] Lozano, P., "Ionic Liquid Ion Sources: Suppression of Electrochemical Reactions using Voltage Alternation," Journal of Colloid and Interface Science, 280(1), 149-154 (2004).
[12] Brikner, N., Lozano, P., "The role of upstream distal electrodes in mitigating electrochemical degradation of ionic liquid ion sources," Applied Physics Letters, 101(19):193504, 2012
[13] Krejci, D., Mier-Hicks, F., Fucetola, C., Lozano, P., Hsu-Schouten, A., Martel, F., "Design and Characterization of a Scalable ion Electrospray Propulsion System," IEPC-2015-149, Hyogo-Kobe, Japan.
[14] Krejci, D., Mier-Hicks, F., Thomas, R., Haag, T., Lozano, P, "Emission Characteristics of Passively Fed Electrospray Microthrusters with Propellant Reservoirs," Journal of Spacecraft and Rockets, 54(2) (2017) 447-458.
[15] Hsu-Schouten, A., Beiting, E., Curtiss, T., "Performance of a Torsional Thrust Stand with 1 μN Sensitivity," IEPC-2015-90062, Hyogo-Kobe, Japan.
[16] J. Rojas-Herrera, C. Fucetola, D. Krejci, D. Freeman, I. Jivanescu and P.C. Lozano, "Porous materials for ion-electrospray spacecraft micro-engines, Nanomechanics and Micromechanics," 2017, 7(3)

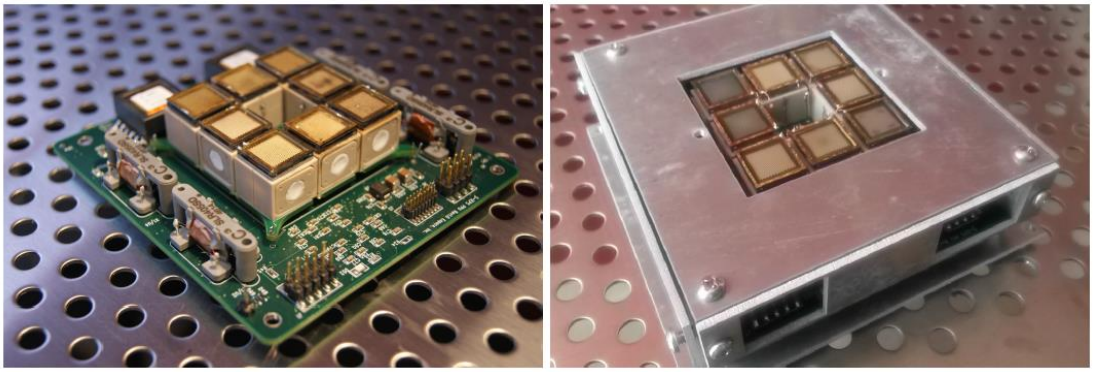

Figure 1. S-iEPS propulsion module with 8 thrusters aligned along a single axis [14].

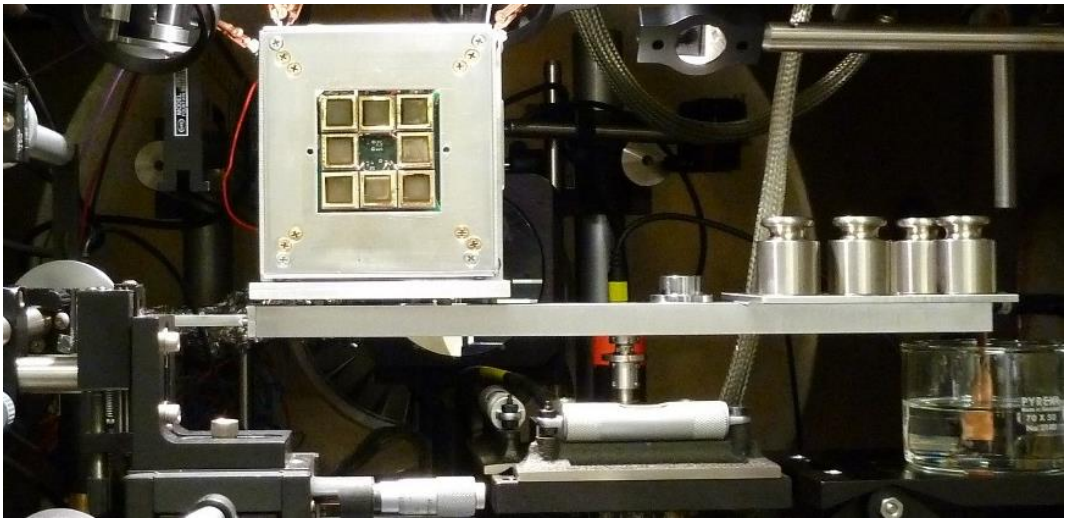

Figure 2 Photo of the S-iEPS unit mounted to the thrust stand, ready for testing.

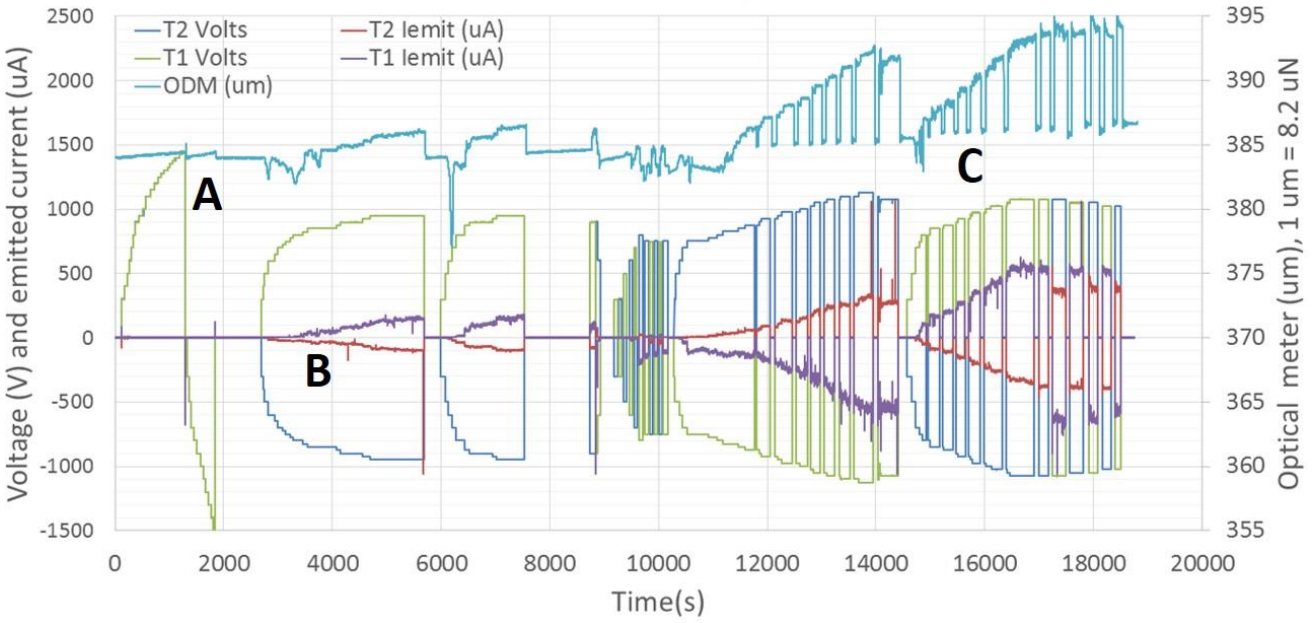

Figure 3. Thruster warm-up performed on 06/19/2015.

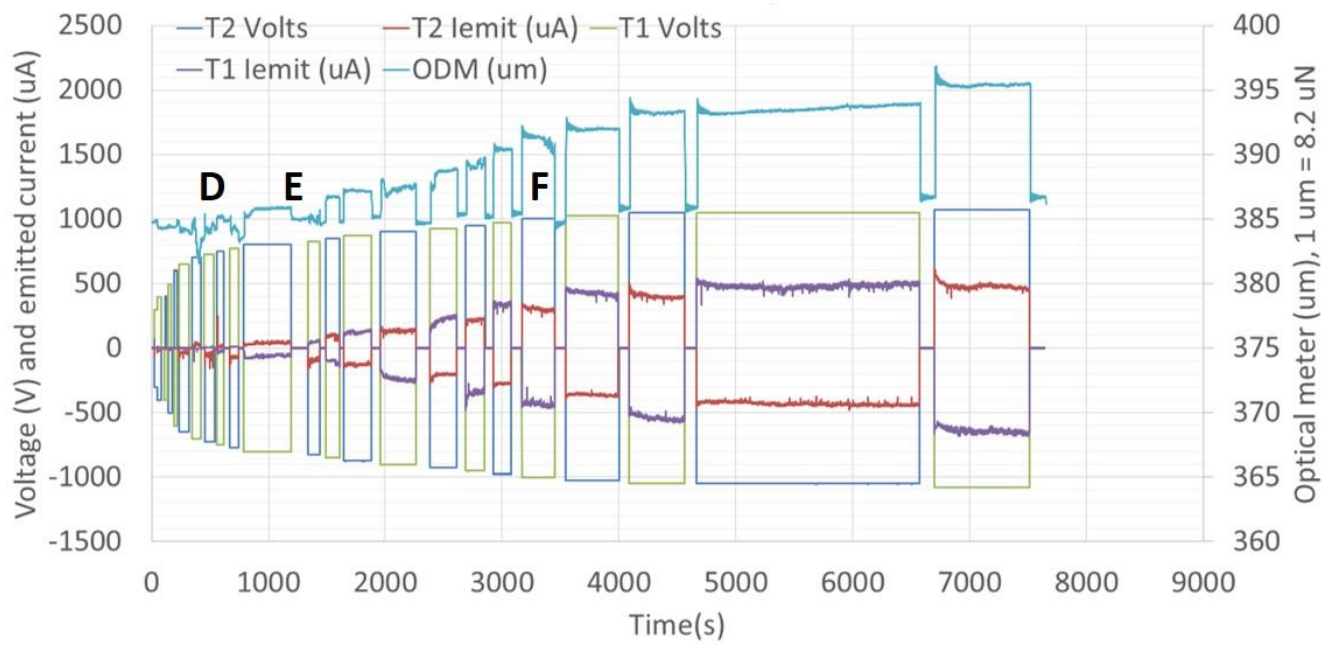

Figure 4. Thruster warm-up continued on 06/20/2015 (manual switching mode).

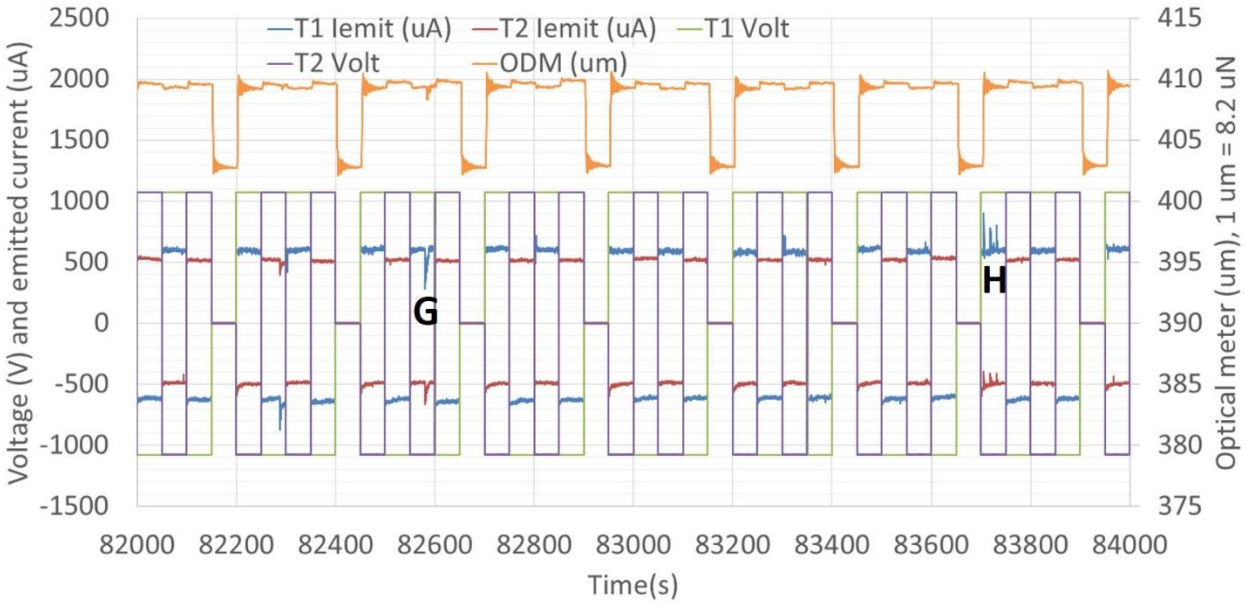

Figure 5. Thruster performance stabilizing at +/- 1075V, producing ~57 µN thrust.

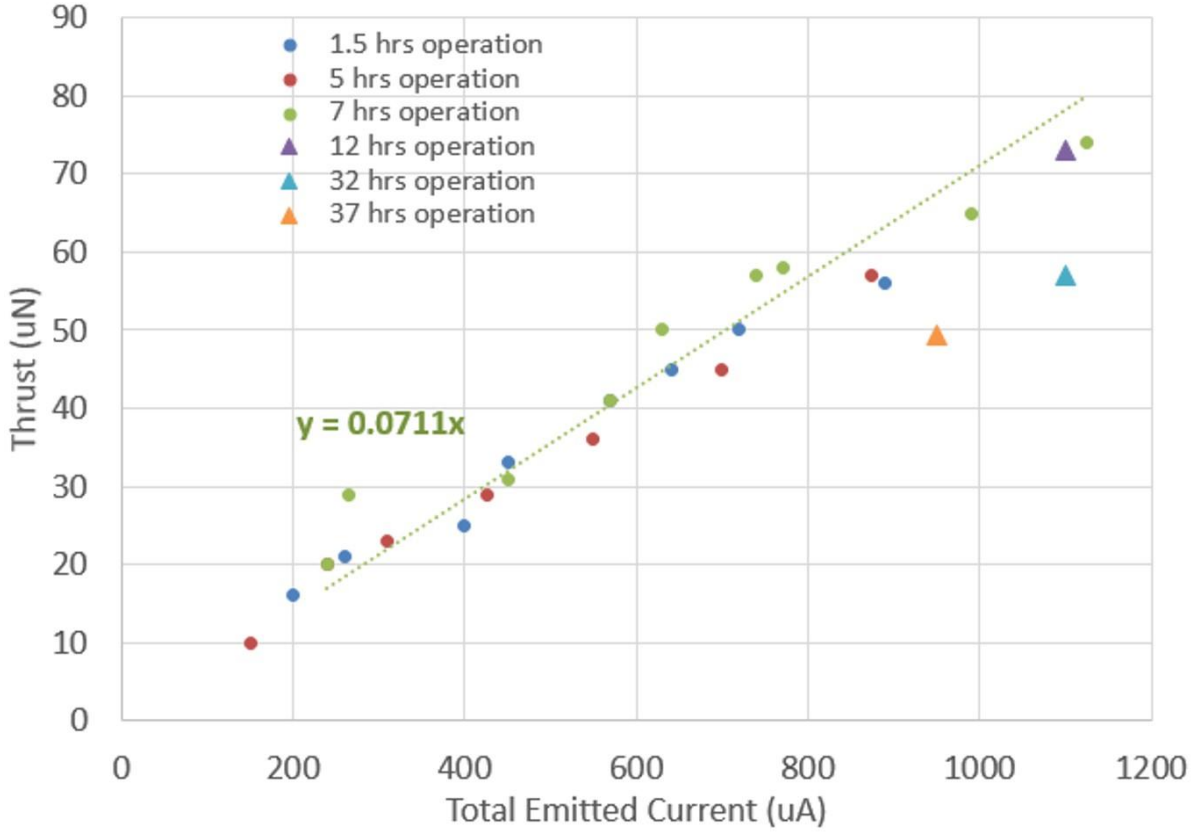

Figure 6. Thrust vs. total emitted current

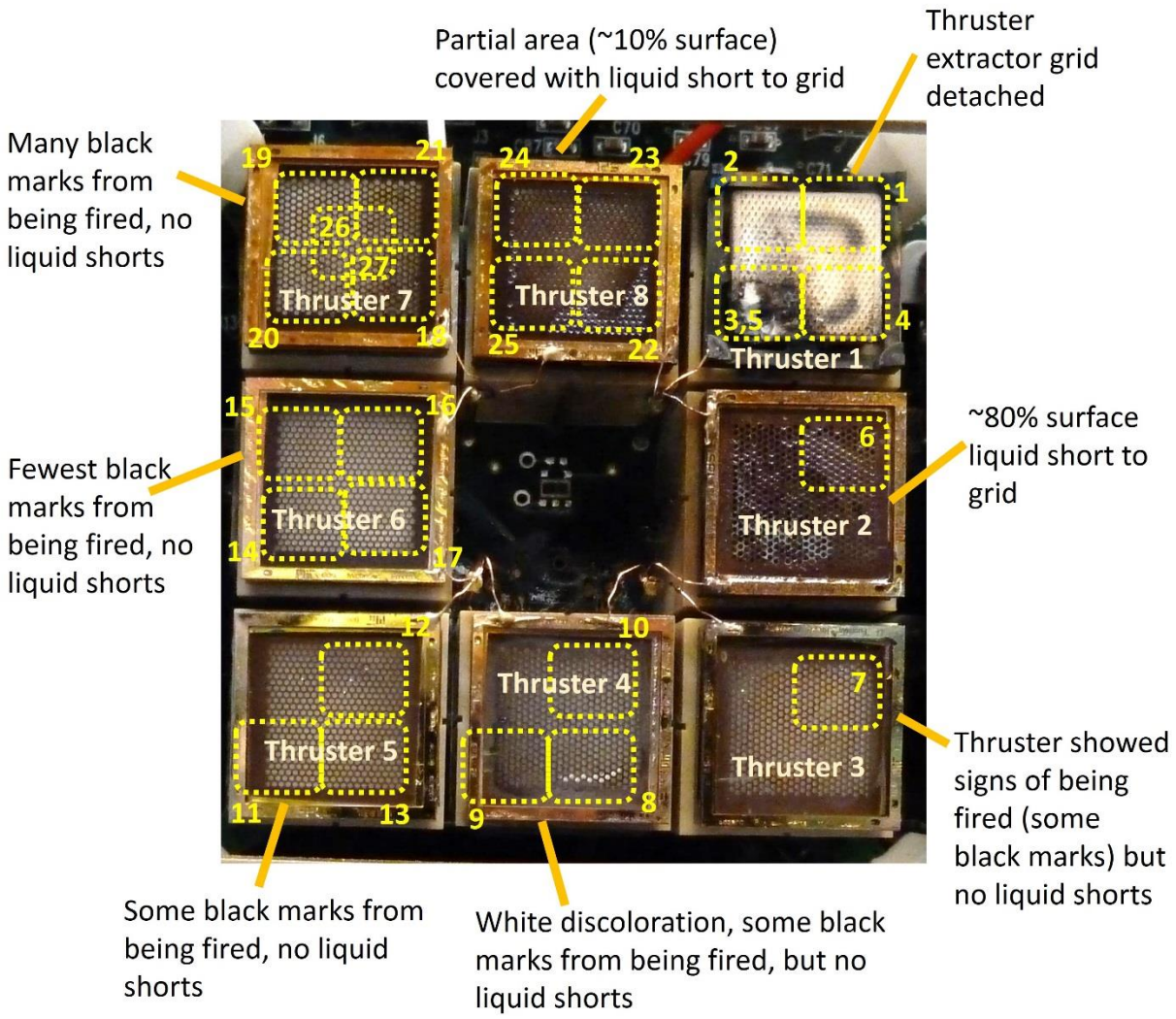

Figure 7. Post-life thruster inspection

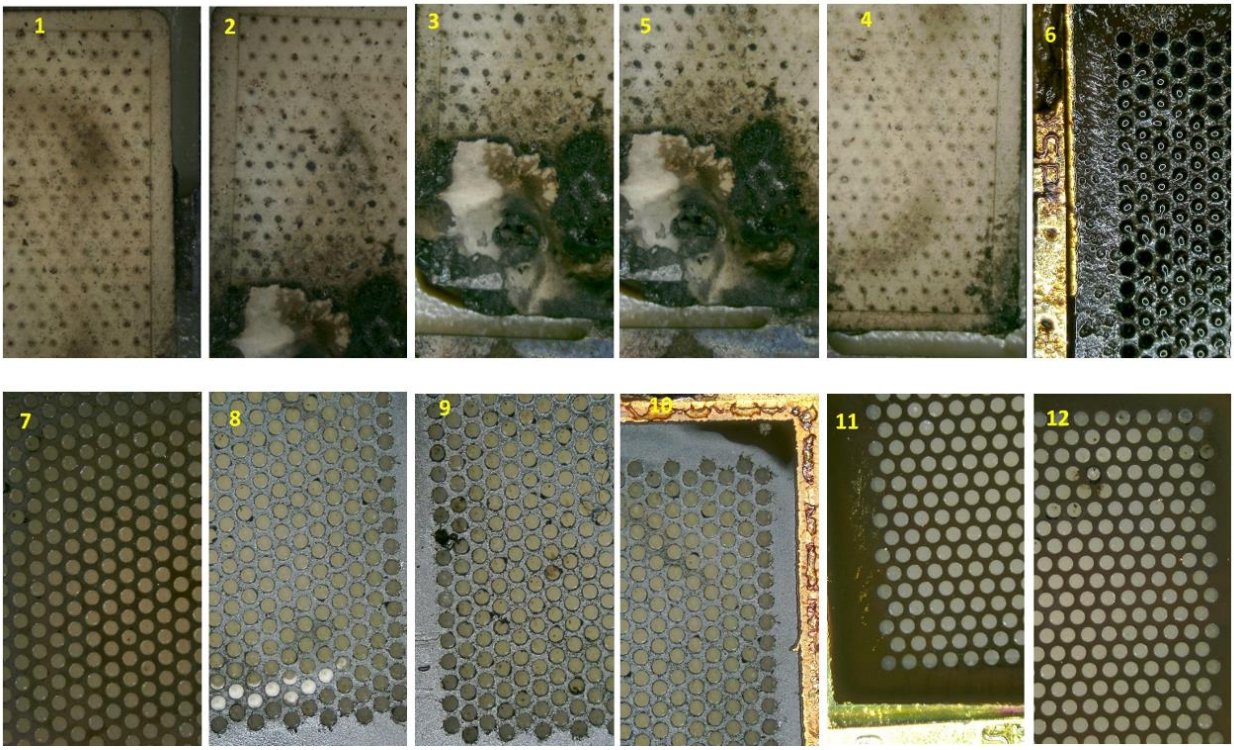

Figure 8. Closeups of post-life visual inspection (1 of 2)

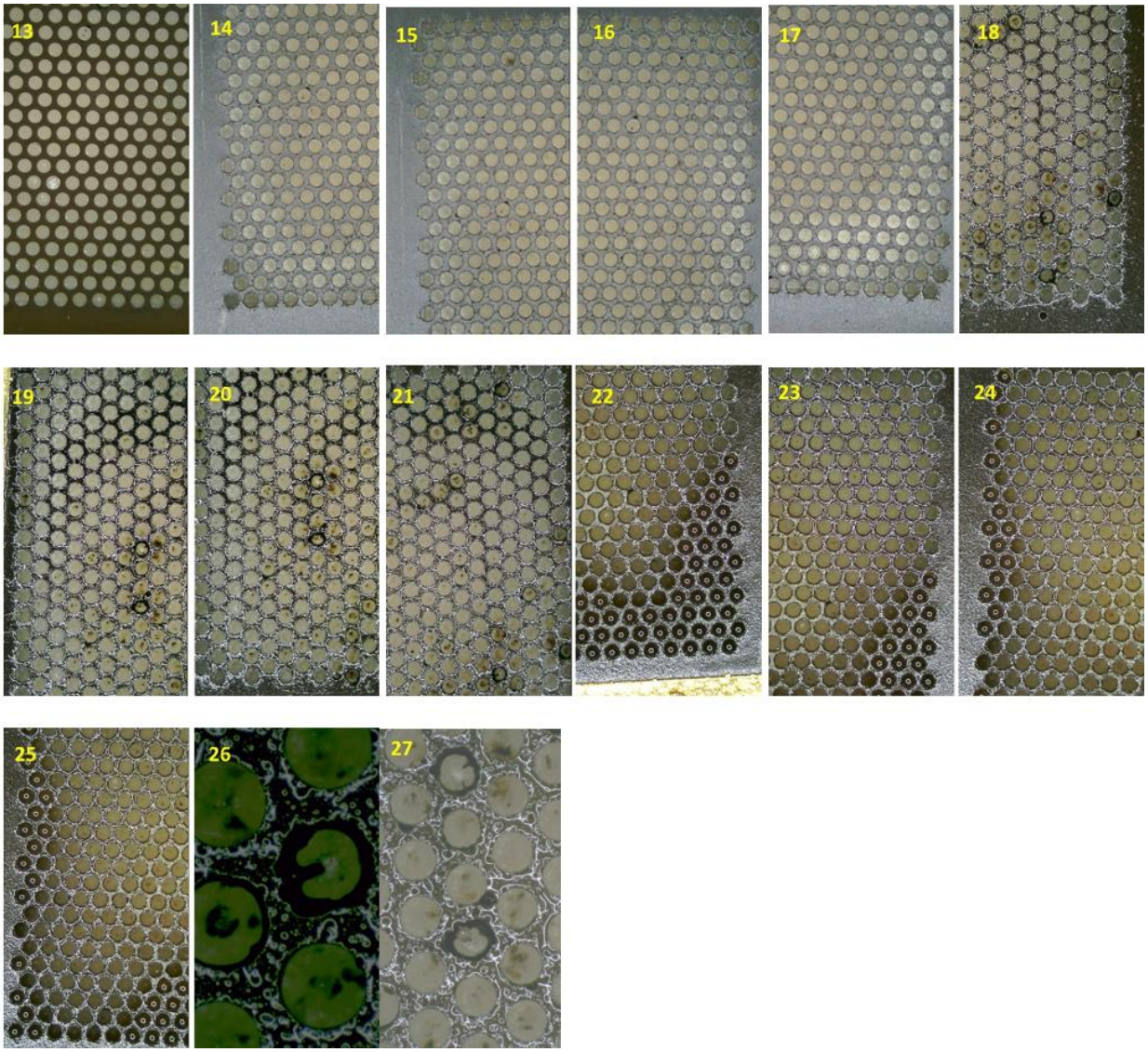

Figure 9. Closeups of post-life visual inspection (2 of 2)